Combined photoemission and inverse photoemission study of HfS$_2$

M. Traving, T. Seydel, L. Kipp,* and M. Skibowski

Institut für Experimentelle und Angewandte Physik, Universität Kiel, D–24098 Kiel, Germany

F. Starrost, E. E. Krasovskii, A. Perlov,† and W. Schattke

Institut für Theoretische Physik, Universität Kiel, D–24098 Kiel, Germany

We report on a comprehensive study of the electronic structure of the layered semiconductor $1T$-HfS$_2$. The occupied and unoccupied band structure has been investigated by combined angle-resolved photoemission and inverse photoemission. The results are discussed in the context of a fully relativistic linear-muffin-tin-orbital calculation as well as an extended linear-augmented-plane-wave calculation showing a very good agreement between experiment and theory. From the measurements, we obtain an indirect band gap of 2.85 eV between Γ and M/L. This value differs significantly from optical results (≈ 2 eV). In the normal direction we observe the direct band gap of 3.6 eV.

PACS number(s): 79.60.−i, 71.20.−b, 71.15.Ap

I. INTRODUCTION

There has been a number of experimental and theoretical investigations of the geometric and electronic structure of the transition-metal dichalcogenides.[1–5] Especially, semiconductor heterojunctions of layered materials grown by van der Waals epitaxy showing nearly defect-free interfaces (van der Waals epitaxy) led to an increasing interest in the last years.[6,7] For the understanding and the improvement of the heterojunction properties, it is important to have an accurate picture of the electronic structure of the layered semiconductors.

In the case of HfS$_2$, the determination of the electronic properties is partly still incomplete. According to optical experiments,[8–10] HfS$_2$ has an indirect band gap of about 2 eV. The band structure has been calculated by several methods. All theoretical results give an indirect band gap. Fong *et al.*[11] (empirical pseudopotential method) and Bullett[12] (atomic-orbital method) get a fundamental band gap of about 1.9 eV, Murray *et al.*[13] (semiempirical tight-binding method) and Mattheiss[14] [nonrelativistic augmented plane-wave (APW) method] predict a fundamental gap of about 2.7 eV. They all find the valence-band maximum at the Γ point and the conduction-band minimum at the *L* point (Fong *et al.* at the *M* point). Jakovidis *et al.*[15] determined the band structure of HfS$_2$ in the Γ*M* direction by angle-resolved photoemission spectroscopy and discussed it in the context of the theories of Bullett[12] and Mattheiss.[14] To our knowledge there exists no work about the unoccupied band structure of HfS$_2$.

In this paper we present a complete study of the valence- and conduction-band structure of HfS$_2$. The experimental band structure and the band gap were investigated by means of combined angle-resolved photoemission and inverse photoemission spectroscopy (CARPIP).[16] The experimental results will be compared with band-structure calculations using the relativistic linear-muffin-tin-orbital (RLMTO) method for the occupied bands and the extended linear-augmented-plane-wave (ELAPW) method for the unoccupied states.

The schematic description of the structural and electronic properties of HfS$_2$ in Sec. II is followed by details about the experimental setup (Sec. III). Afterwards we will focus on the experimental determination of the valence-band maximum (VBM) and conduction-band minimum (CBM) (Sec. IV). In the subsequent Sec. V, we will describe the band-structure calculations and make conclusions about their results. Finally, a comprehensive discussion of the experimental valence- and conduction-band structure will be presented and compared with theory in Sec. VI.

II. STRUCTURAL AND ELECTRONIC PROPERTIES

Due to the layered structure of the transition-metal dichalcogenides, their macroscopic and microscopic properties exhibit a pronounced two-dimensional character. This striking anisotropic structure results from the strong ionic and covalent intralayer bonding and the weak van der Waals-like interlayer bonding. Hence, we can observe a strong anisotropic behavior in, e.g., optical and electronic properties among the transition-metal dichalcogenides.

One layer consists of one-layer plane of hexagonal close-packed Hf atoms sandwiched by two-layer planes of also hexagonal close-packed S atoms. The Hf atom is octahedrally coordinated by the chalcogen atoms [Fig. 1(a)]. HfS$_2$ adopts the CdI$_2$ structure (1T structure) with the corresponding space group $P\bar{3}m1$. Therefore, the lattice constant c is spanned by only one sandwich layer. The lattice parameters are $a = 3.635$ Å^{-1} and $c = 5.837$ Å^{-1} (from Ref. 5). Figure
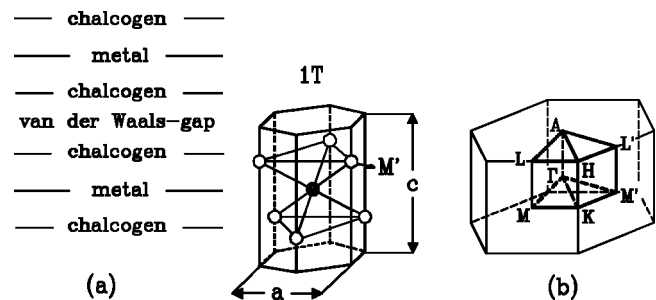

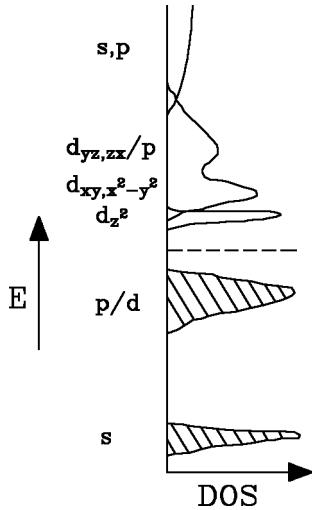FIG. 1. (a) Coordination of the S atoms in $1T$-HfS$_2$ (according to Wilson and Yoffe Ref. 2), (b) Brillouin zone of HfS$_2$.

FIG. 2. Schematic view of the electronic band structure of HfS_2 (according to Liang Ref. 1).

1(b) shows the corresponding Brillouin zone of HfS_2. Capitals denote points of high symmetry.

The schematic density of states suggested by Liang[1] gives a rough picture of the electronic structure of transition-metal dichalcogenides (Fig. 2). The energetically lowest valence-band states show mainly $S4s$ and $S4p$ character. Since for group IVB transition-metals the intralayer bonding shows about 30% ionic character, the octahedral coordination is favored. The resulting band gap depends strongly on the actual materials. The following cationlike d states can be divided into the bands showing t_{2g} symmetry (d_{z^2}, $d_{x^2-y^2}$, d_{xy}) and the bands with e_g symmetry (d_{xz}, d_{yz}). The main contribution of the antibonding s and p states arises from the cation.

III. EXPERIMENT

The angle-resolved photoemission spectra were taken with the angle-resolved photoelectron spectroscopy (ARPES) experiments at the HONORMI beamline of the DORIS III storage ring at Hamburg Synchrotron Radiation Laboratory (HASYLAB) (photon energy range $9\,\text{eV} < h\nu < 33$ eV) and in Kiel using a He discharge lamp ($h\nu = 21.22$ eV). The electron detection was performed by a $180°$ spherical analyzer mounted on a goniometer that can be driven around two independent axes. By these two degrees of freedom, we get the final sample adjustment with high accuracy by taking spectra in small angle steps around the critical points without moving the sample. The spectra illustrated in this paper show an angle resolution $\Delta\vartheta < 0.25°$ and an overall energy resolution of $50\,\text{meV} < \Delta E < 130$ meV using synchrotron radiation, and $\Delta E = 65$ meV using He I_α excitation.

The inverse photoemission spectra were taken by using a compact grating spectrometer with parallel detection of photons in the energy range of $10\,\text{eV} \leq h\nu \leq 40$ eV in discrete channels g_k.[17,16] As electron source we used an electron gun of the Erdman-Zipf type.[18] The focus of the electron beam on the sample is about 1 mm^2 spot size and has an angle divergence of less than $3°$. Energy and momentum resolu-

tions are typically 400 meV and 0.05 Å^{-1}.

To determine the electronic transitions from the spectra, the inverse photoemission data have been deconvoluted by a maximum entropy algorithm.[19,20] A Gaussian resolution function with full width at half maximum (FWHM) depending on the energy of incidence eU_0 has been assumed varying from 360 meV FWHM at $eU_0 = 11$ eV to 800 meV FWHM at $eU_0 = 27$ eV. Noise has been taken into account by the assumption $\Delta_k = \alpha + \beta\sqrt{g_k}$ with g_k being the intensity in channel k of the channel plate and constants α, β adapted to the experimental conditions. The maxima in the deconvoluted spectra have been identified as the electronic transitions. This approach is more precise than an ambigious fit of the broad non-Gaussian peaks in the original spectra. The photoemission spectra with their much better resolution were directly fitted by Gaussian peaks.

Concerning semiconductors like HfS_2, the energy is usually referred to the valence-band maximum (VBM). By the combination of the angle-resolved photoemission and inverse photoemission (CARPIP) spectroscopy we get a common energy scale for both spectroscopies.[16] This is achieved by detecting the electron energy from the inverse photoemission electron gun with the photoemission electron energy analyzer. In this way, the Fermi level becomes obsolete as reference energy and band-bending effects are eliminated. Therefore, CARPIP is the ideal tool for investigation of the occupied and unoccupied band structure with high accuracy, especially of the fundamental band gap.

The samples used in these experiments were grown by chemical vapor transport using iodine as transport gas. They were stuck to the sample holder by silver containing epoxy glue. By cleaving the crystals parallel to the sandwich layers we obtained clean surfaces in the ultrahigh vacuum ($\sim 10^{-10}$ mbar). The orientation of the crystallographic axes was determined by Laue x ray diffraction. The crystal quality was characterized by low-energy electron diffraction, scanning tunneling microscopy, and the surface sensitivity of photoemission and inverse photoemission itself.

IV. DETERMINATION OF VBM AND CBM

In the case of semiconductors, the energies usually are referred to the valence-band maximum (VBM). Thus, for the discussion of experimental results together with band-structure calculations, it is important to have a precise experimental determination of the VBM. An appropriate tool for this purpose are investigations by means of angle-resolved photoemission spectroscopy in combination with synchrotron radiation.[21–24]

The spectra in Fig. 3(a) were taken in the energy distribution curve (EDC) mode, i.e., at constant photon energy the kinetic energy of the detected electrons is scanned. By changing the photon energy as a parameter the $k_\perp$ components in the EDC spectra can be changed. The VBM then turns out as the emission feature highest in energy.

As shown in Sec. VI, we find that the energetically highest peak in the $\Gamma M(AL)$, as well as in the $\Gamma K(AH)$, direction disperses towards higher binding energies for increasing polar angle ϑ, respectively. As predicted by theory (Sec. V),
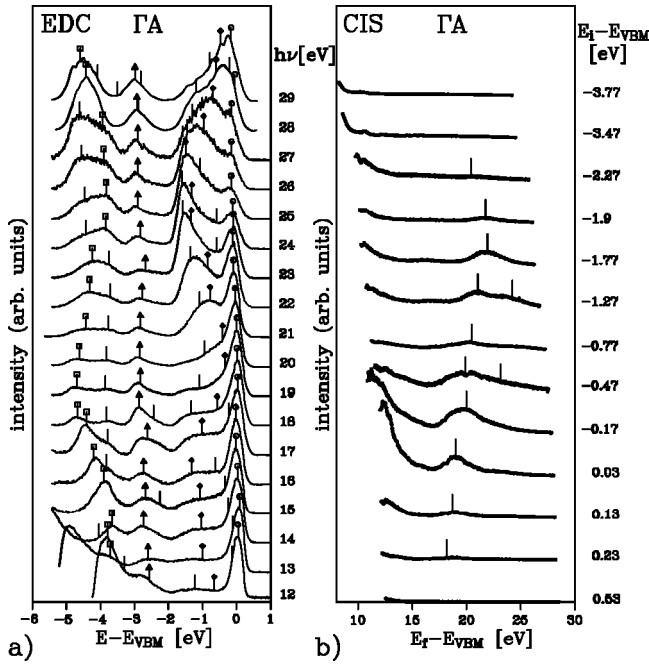
FIG. 3. (a) Normal emission photoelectron spectra of HfS_2 taken in the EDC mode. Strong emissions are marked by symbols. (b) Normal emission constant initial state (CIS) photoelectron spectra.

FIG. 4. Valence-band structure along ΓA as derived from the spectra in Fig. 3.

we therefore expect the VBM in the normal direction (ΓA direction).

To take into account $k_\perp$ effects along ΓA we have taken normal emission ($k_\parallel = 0$) EDC spectra at different photon energies and constant initial energy spectra (CIS) for different initial energies (Fig. 3). The energetically highest valence band marked by circles shows nearly no dispersion. Because of the weak van der Waals interaction between the layers, one would expect nearly no dispersion of the bands perpendicular to the layers as verified for WSe_2.[24] However, besides two nearly dispersionless valence-band peaks (circles and triangles) in Fig. 3(a), we observe energy bands showing distinct dispersion (rhombus and squares) as generally found for the 1T materials. This is also observed in the CIS spectra of Fig. 3(b) where a distinct dispersion of the final states between 18 and 22 eV appears.

For the determination of the $k_\perp$ component, we discuss the spectra in Fig. 3(a) in the context of the ELAPW calculation (Fig. 9 in Sec. V). For the final states of the photoelectrons we assume free electronlike dispersion. Figure 4 shows the comparison of the band structure of experiment and theory (ELAPW) in the ΓA direction. For an inner potential $V_0 = 4.5$ eV and two reciprocal-lattice vectors folding back the experimental valence-band structure into the reduced Brillouin zone, a reasonable agreement between theory and experimentally determined transitions is obtained.

The energetical positions of the bands A and C from theory are in very good agreement with the two dispersionless bands (circles and triangles). The dispersive band (rhombus) can be identified with the theoretical band between 0 and 2.4 eV binding energy (B). At the zone center Γ, these two bands (A,B) overlap slightly. This behavior can be ob-
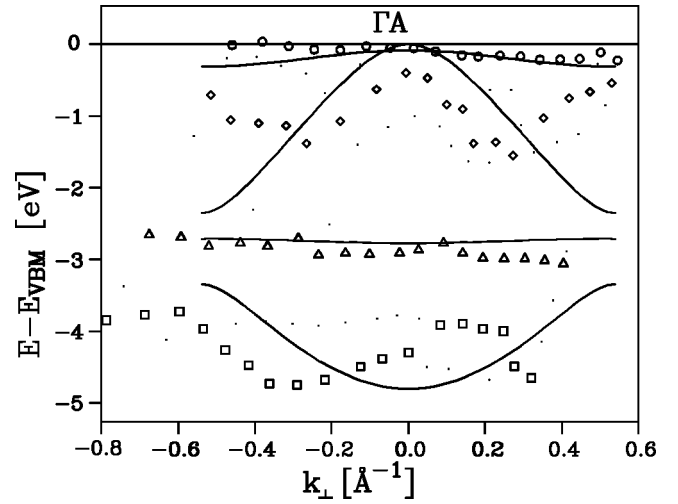
served in the EDC spectrum taken at $h\nu = 19$ eV photon energy. Therefore, by use of the theoretical band structure we find the valence-band maximum at the Γ point, i.e., the center of the Brillouin zone.

The conduction-band minimum is investigated by means of CARPIP. This method provides a common unique energy scale for the spectra of photoemission and inverse photoemission independent of the Fermi energy. In this way we
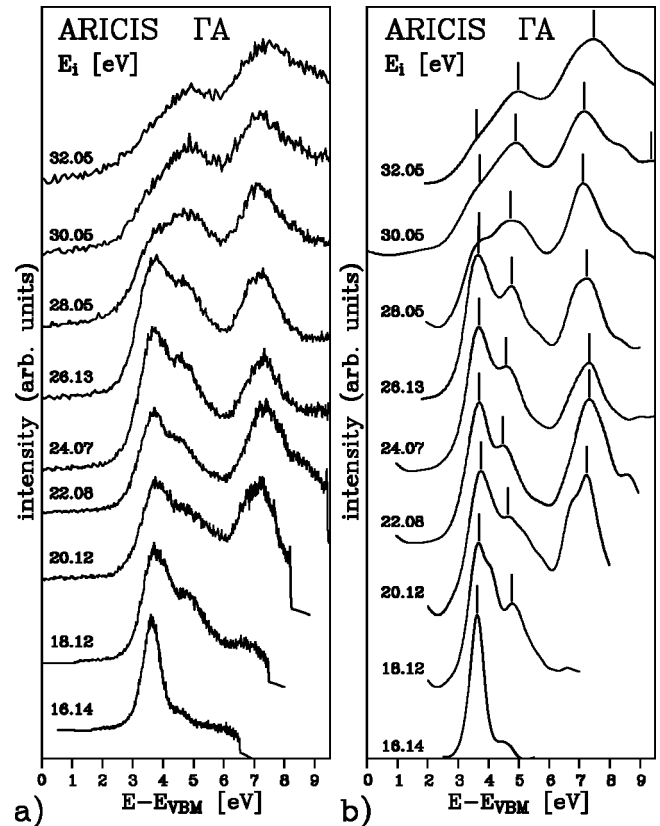

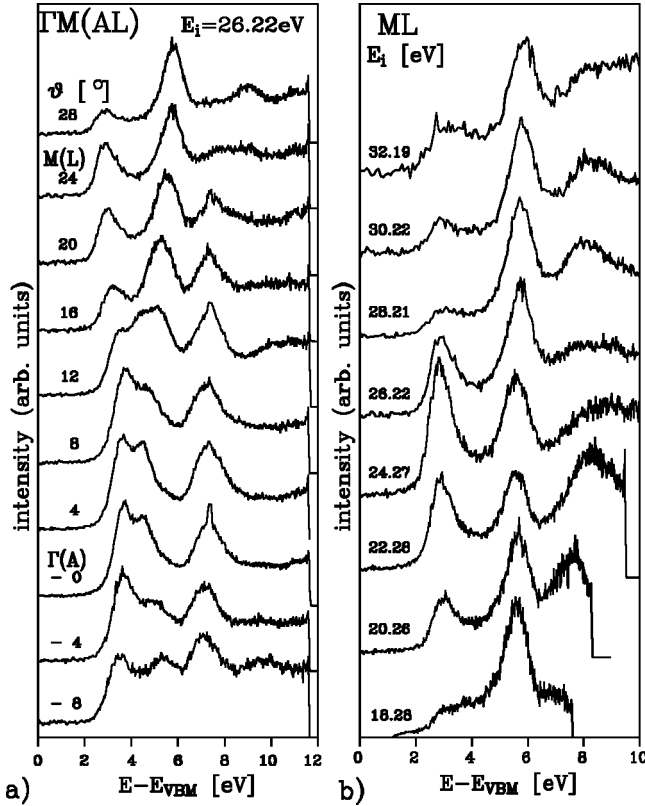FIG. 5. (a) ARICIS spectra in ΓA direction ($k_\parallel = 0$). (b) Maximum entropy deconvolution of (a).

FIG. 6. ARICIS spectra along ΓM taken at an initial electron energy of 21 eV (a) and along ML (b).

FIG. 7. Direct and indirect band gap of HfS_2 as derived from the measurements in Figs. 3, 5, and 6.

get **k**-resolved information about the band gap.

The spectra of the unoccupied states are taken in the angle-resolved inverse constant initial energy spectroscopy (ARICIS) mode, i.e., at constant electron energy the spectrometer detects the photon spectrum. Therefore the $k_{\parallel}$ component of the peaks is constant in the whole spectrum in contrast to EDC spectra in ARPES.

In Fig. 5, ARICIS spectra taken for a normal incident electron beam are shown. Upon changing the electron energy, the $k_{\perp}$ component is varied along ΓA direction of the Brillouin zone (perpendicular to the layers). At about 3.6 eV above the VBM, we observe a nearly nondispersive peak. With increasing polar angle ϑ in ΓM direction, the peak disperses towards lower energies [Fig. 6(a)]. At $M(L)$, this band is running through a minimum. Figure 6(b) presents ARICIS spectra taken in the ML direction at different electron energies. The lowest conduction band shows a pronounced intensity modulation, but nearly no dispersion. Thus, we find the conduction-band minimum in the ML direction in line with the ELAPW calculation, which places the CBM at L (Fig. 9).

Therefore, the observed fundamental band gap is indirect and has a value of 2.85 eV (Fig. 7). The direct band gap we observe in the normal direction (3.6 eV). On the other hand, optical measurements result in a smaller band gap (≈ 2.0 eV and 1.96 eV)[25] (Greenaway *et al.*[10]) than CARPIP shows. The energy difference in the determined band gaps probably arises from exitonic effects involved in optical measurements.
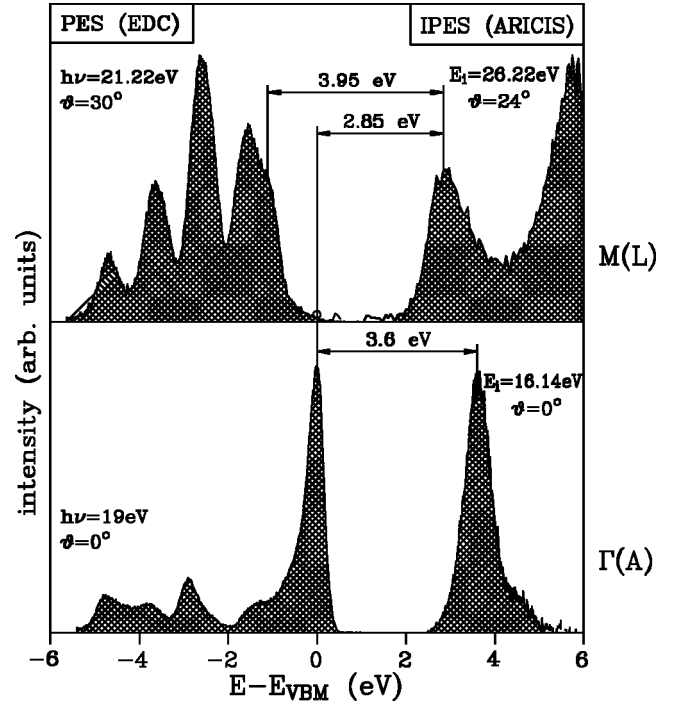
V. BULK BAND-STRUCTURE CALCULATION

The bulk band structure of HfS_2 was calculated self-consistently within the local-density approximation using two techniques. For the valence bands, the fully relativistic linear-muffin-tin-orbital (RLMTO) method[26,27] was used, while for the conduction bands the scalar-relativistic extended linear-augmented-plane-wave (ELAPW) method[28] was applied. The ELAPW method is accurate even for higher unoccupied energies because of the extended radial basis set.[29] For both methods, an atomic basis of three atoms and one empty sphere were used, as in Ref. 12 with $z = 0.25$.

For the RLMTO calculations, basis functions were used that included angular momenta up to $l = 3$ for Hf, $l = 2$ for S, and $l = 1$ for the empty sphere. Non-atomic-sphere approximation (ASA) contributions to the overlap matrix were taken into account, i.e., the so-called combined correction was used.[30] The ELAPW set of basis functions was made up of all APW's with reciprocal-lattice vectors $\vec{G}$ for which $|\vec{G}|S < 9.6$, where $S = 2.418$ a.u. is the radius of all the muffin-tin spheres. There were 487 usual APW basis functions and 64 extension functions.

Since the layered crystal HfS_2 has an inert (0001) surface, no surface states are expected and only the bulk band structures have been determined. The valence-band structure, as well as an extended range of the conduction-band structure, were calculated since for the construction of electron-transition (ET) plots the knowledge of the final states is necessary. The ET plots assist in the identification of electron transitions in theory and experiment. As long as no calculations within the one-step model of photoemission are
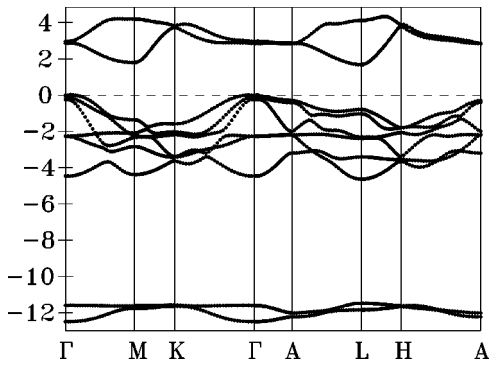
FIG. 8. Band structure of HfS$_2$ calculated by the fully relativistic RLMTO method. The valence-band maximum is chosen as the energy zero.

FIG. 10. Electron transition plot of the valence bands in the ΓA direction of HfS$_2$. Symbols represent the experimental data, lines, the theoretically possible photoemission transitions using the RLMTO calculation for the valence bands, and the ELAPW calculation for the conduction bands.

available, ET plots are indispensable for reliable statements on the band structure.

The electron transition plots (see Figs. 10 and 11) are derived from the LMTO valence bands (Fig. 8) and ELAPW conduction bands (Fig. 9). The overwhelming amount of ELAPW final state bands that are far from a simple parabolic behavior should be mentioned. The valence band part is only shown for comparison and completeness. Focusing on the ΓA direction, free electronlike branches folded back at the zone boundaries appear for high energies, besides a series of gaps and less dispersive bands below 15 eV. Parts of the free electronlike bands are mainly associated with wave vectors
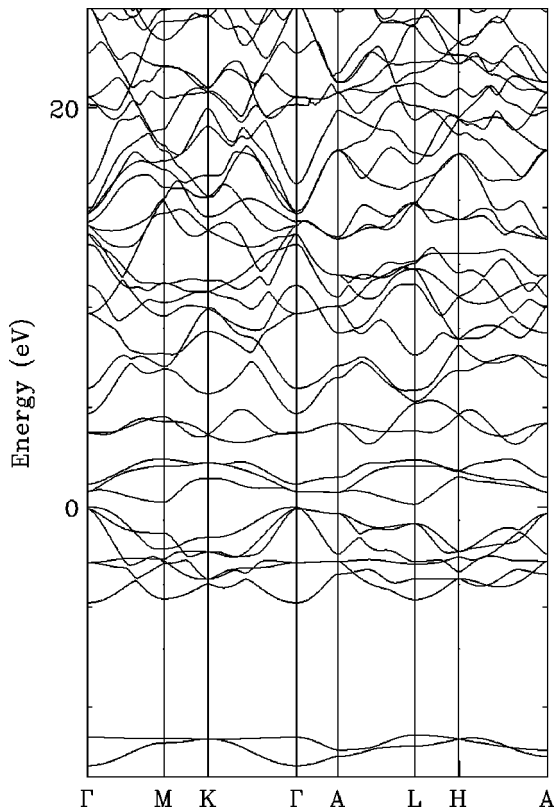
perpendicular to the layer planes only. However, in contrast to the well-known normal emission finding that forward emission often dominates the photocurrent, here we could not detect such a behavior. Rather, the electron transition plots to be discussed in the following show that the electron emissions accumulate rather from the regions of high one-dimensional density of states as given by the band edges or by the low-dispersive bands.

In the RLMTO calculation, as well as in the ELAPW calculation, we find the VBM at the Γ point and the CBM at the L point, so that in agreement with experiment an indirect band gap results. The lowest unoccupied bands at M and L show hardly any dispersion [in line with Fig. 6(b)]. Consequently, from the theoretical point of view, we cannot decide whether the CBM is at M or L. Since the exchange-correlation potential is treated within the local-density approximation, we encounter in our band-structures the well-known effect that the gaps between occupied and unoccupied bands are too small when compared to the experimental results.

FIG. 9. Band structure of HfS$_2$ (dots and lines) calculated by the scalar-relativistic ELAPW method. The valence-band maximum is chosen as the energy zero.

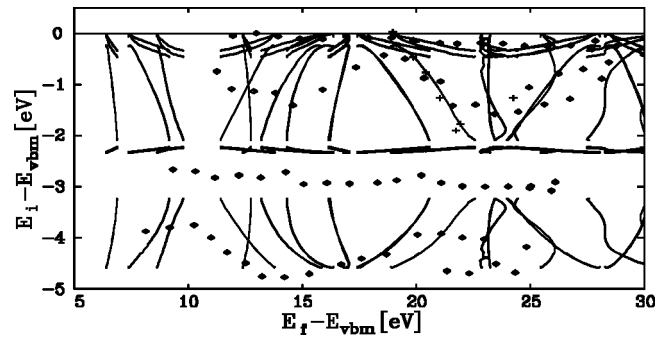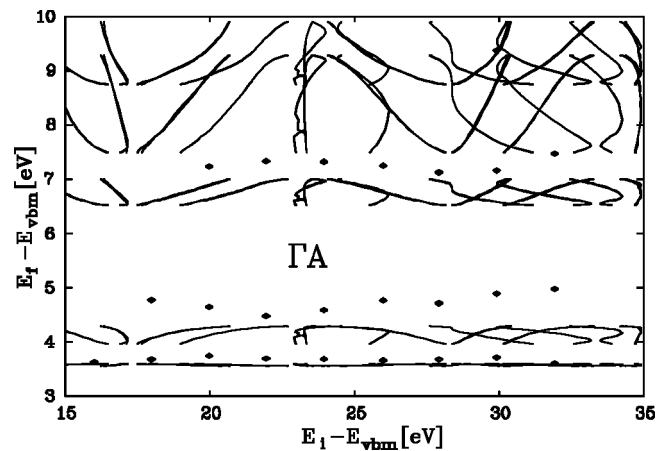FIG. 11. Electron transition plot for conduction bands showing transitions from unoccupied states in the ΓA direction of HfS$_2$. Solid lines represent theoretically possible transitions. Experimental data are plotted by symbols. The theoretical states are shifted by 2.69 eV. E_i and E_f denote the energy of the initial and final state, respectively.
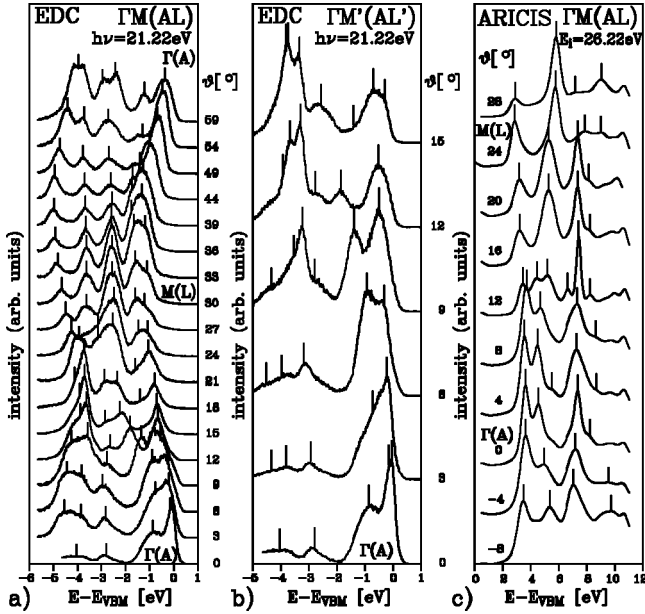
FIG. 12. (a) EDC spectra in $\Gamma M(AL)$ direction for photon energy $h\nu = 21.22$ eV. (b) EDC spectra in $\Gamma M'(AL')$ direction for photon energy $h\nu = 21.22$ eV. (c) Maximum entropy deconvolution of the ARICIS spectra in $\Gamma M(AL)$ direction of Fig. 6.

FIG. 13. Comparison of the occupied and unoccupied band structure in $\Gamma M(AL)$ direction with a projection of the RLMTO calculation (Fig. 8) and the ELAPW calculation (Fig. 9).

VI. RESULTS AND DISCUSSION

A. Electronic structure along ΓA

For the investigation of the electronic structure in the ΓA direction EDC and CIS spectra, as well as ARICIS spectra, were taken perpendicular to the layers (Sec. IV). At the surface, i.e., the bulk-vacuum interface, the periodicity of the bulk crystal is terminated. Consequently, the $k_\perp$ component of the wave vector $\vec{k}$ in photoemission spectroscopy (PES) and inverse PES (IPES) is unknown.

There exist two possibilities to compare experimental and theoretical results in this direction. In the case of photoemission, the final-state dispersion can be approximated by parabolas (inverse photoemission, vice versa). From the transitions we can determine the $k_\perp$. The result of this procedure is shown in Fig. 4. The second possibility makes use of the electron transition (ET) plot where initial-state energies are plotted against final-state energies (experiment and theory). In this way, the $k_\perp$ problem can be avoided.

In the case of the theoretical valence-band structure, all possible photoemission transitions between the occupied states of the RLMTO calculation and the unoccupied states of the ELAPW calculation were considered and plotted in the graph omitting selection rules (Fig. 10). The final-state bands in the ELAPW calculation were shifted by $\Delta E = 2.69$ eV to higher energies resulting in a band gap in line with experiment. In the same way, experimental peaks were plotted in the graph. All energies are referred to the VBM.

At $E_i - E_{VBM} \approx -0$ eV and $E_i - E_{VBM} \approx -2.5$ eV, we observe transitions whose initial-state bands show nearly no dispersion, respectively (Sec. IV). At $E_i - E_{VBM} \approx -0$ eV the highest (in theory twofold degenerate) valence band including the VBM is involved. The other band is also twofold
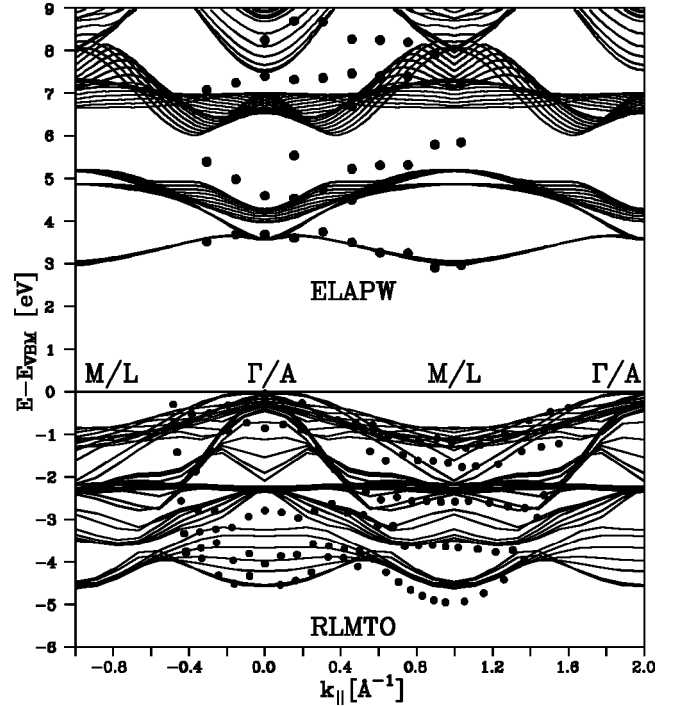
degenerate where the theoretical band appears 0.5 eV above the strong emission at $E_B = -2.8$ eV. In addition, in photoemission we observe two dispersive structures between $E_B = -4.8$ and -3.8 eV as well as between $E_B = -1.7$ and -0.4 eV partly showing good agreement with theoretical transitions. Especially, at $E_i - E_{VBM} = -2.8$–0 eV and $E_f - E_{VBM} = 18$–22 eV, the transition in theory fits well with the transitions in EDC (rhombus) and CIS spectra (crosses).

Concerning the transitions between conduction bands, the initial states, as well as the final states were taken from the ELAPW calculation. The comparison of the transitions in experiment and theory is shown in the ET plot in Fig. 11. We observe a good agreement in binding energy ($E_f - E_{VBM}$) of the three lowest, nearly dispersionless, emissions with theory.

B. Electronic structure along $\Gamma M(AL)$

For the determination of the electronic structure in $\Gamma M(AL)$ and $\Gamma K(AH)$ direction we took off-normal emission EDC spectra at $h\nu = 21.22$ eV and off-normal incidence ARICIS spectra at $E_i = 26.1$ eV.

In Fig. 12(a) EDC spectra in $\Gamma M(AL)$ and $\Gamma M'(AL')$ direction are shown, respectively. In $\Gamma M(AL)$ direction the polar angle spans from $\vartheta = 0°$ to $\vartheta = 59°$, so that at $E_B = 0$ eV and $\vartheta = 59°$ the Γ point in the second Brillouin zone is nearly passed. This behavior is clearly observable at the highest valence-band emission showing distinct dispersion.

In Fig. 12(c) ARICIS spectra in $\Gamma M(AL)$ direction reconstructed by the maximum entropy method (Sec. II) are shown [The original ARICIS spectra are shown in Fig. 6(a)].
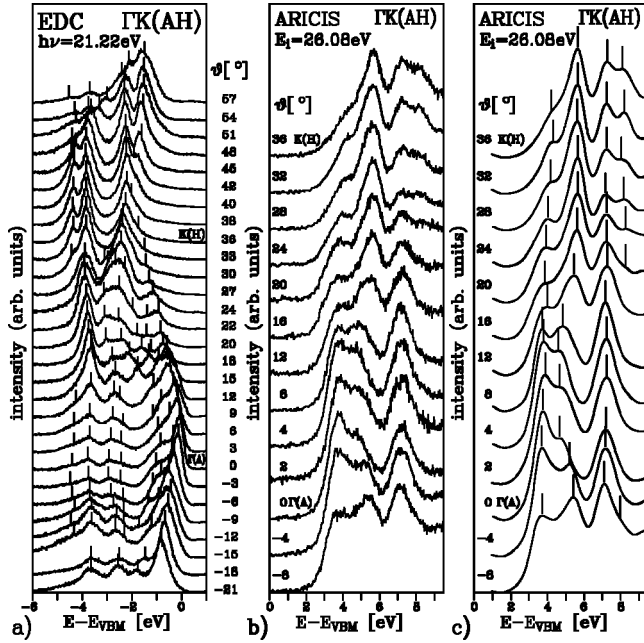
FIG. 14. (a) EDC spectra in $\Gamma K(AH)$ direction for photon energy $h\nu = 21.22$ eV. (b) ARICIS spectra in $\Gamma K(AH)$ direction taken at initial electron energy $E_i = 21$ eV. (c) Maximum entropy reconstruction of these spectra from (b).
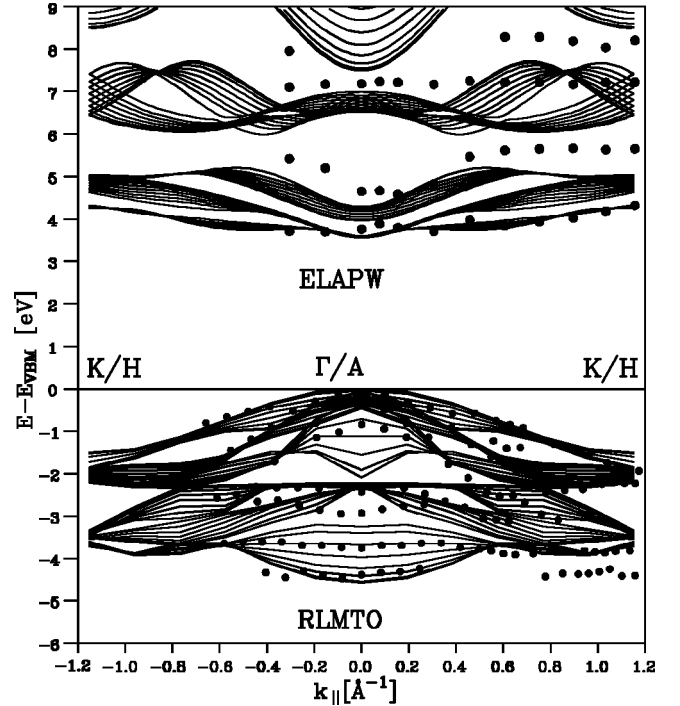

FIG. 15. Comparison of the occupied and unoccupied band structure in $\Gamma K(AH)$ direction with a projection of the RLMTO calculation (Fig. 8) and the ELAPW calculation (Fig. 9).

At normal incidence, the lowest conduction-band emission is 3.6 eV above the VBM. With increasing polar angle ϑ this band disperses towards lower energies until at $\vartheta = 24°[M(L)]$ it becomes the CBM (see Sec. IV).

The comparison between experimental and theoretical band structure in $\Gamma M(AL)$ direction is pictured in Fig. 13. For the occupied states, the RLMTO method was chosen, for the unoccupied states the ELAPW method. Due to the broken symmetry perpendicular to the layers the $k_\perp$ components in the (inverse) photoemission spectra are unknown. Therefore, the peaks determined from the spectra are plotted on a projected band-structure calculation. Since the LDA calculates the band gap much too small, the ELAPW derived bands were shifted by $\Delta E = 2.69$ eV to higher energies.

Generally, there is a very good agreement between experimental and theoretical results. Especially, the dispersion of the highest valence-band emission along $\Gamma M \Gamma$ is in line with theory. Concerning the unoccupied electronic band structure, we observe mainly three distinct emissions that can be identified with bands from the ELAPW calculation. The lowest conduction band is reproduced exactly from theory. According to theory, this band shows nearly no dependence on the $k_\perp$ component and therefore on the initial energy E_i. This is verified by the measurement in ΓA direction (Fig. 5) and the ML direction [Fig. 6(b)]. At $M(L)$ we observe the CBM.

C. Electronic structure along $\Gamma K(AH)$

In this section we investigate the electronic structure in $\Gamma K(AH)$ direction. The theoretical band structure was plotted in the same way as in Sec. VI B for $\Gamma M(AL)$, e.g., RLMTO calculation for the occupied states and ELAPW cal-

culation for the unoccupied states. As in Sec. VI B, we shifted the conduction-band structure by $\Delta E = 2.69$ eV to higher energies. The angle-dependent EDC spectra spans from $\vartheta = -21°$ to $\vartheta = 57°$ [Fig. 14(a)]. Starting at the Γ point ($\vartheta = 0°$) with increasing ϑ one is crossing the K point and then reaching the M point. Fig. 14(b) contains original ARICIS spectra in $\Gamma K(AH)$ direction. The maximum entropy reconstruction of these spectra is given in Fig. 14(c) (Sec. II).

Figure 15 compares experimental and theoretical band structure along $\Gamma K(AH)$. The three highest valence-bands whose individual dispersion can clearly be separated coincide very well with RLMTO. As in ΓA (Fig. 10) and in $\Gamma M(AL)$ direction (Fig. 13) we observe at $E_B = -2.3$ eV a dispersionless band in experiment as well as in theory. The ARICIS spectra yield four emissions that can be associated with theoretical bands, respectively. The lowest conduction band of theory is in very good agreement with the experimental emissions. The remaining experimental conduction bands show about 0.5 eV higher energies than the ELAPW bands do.

VII. CONCLUSIONS

We determined the valence- and conduction-band structure of the semiconducting layered material HfS_2 by means of CARPIP as well as by RLMTO and ELAPW calculations. We applied the maximum entropy method to inverse photoemission data analysis. From the experimental results, we get

an indirect band gap of 2.85 eV. The rather large band gap of 2.85 eV exceeds the value of optical investigations of 2 eV. The difference may probably be attributed to exitonic effects. The VBM is situated at Γ, the center of the Brillouin zone. The CBM is observed in ML direction. The direct band gap of 3.6 eV is found in normal direction. The comparison of experiment and theory along the high-symmetry directions ΓA, ΓM, and ΓK show a convincing agreement for occupied as well as unoccupied states.

---

*Author to whom correspondence should be addressed.

†Present address: Institute of Metal Physics, Ukrainian Academy of Sciences, Vernadskogo 36, 252180 Kiev – 142, Ukraine.

[1] W. Y. Liang, *Electronic Properties of Transition Metal Dichalcogenides and Their Intercalation Complexes*, Vol. 148 of *NATO Advanced Studies Institute* (Plenum, New York, 1986).

[2] J. A. Wilson and A. D. Yoffe, *The Transition Metal Dichalcogenides. Discussion and Interpretation of the Observed Optical, Electrical, and Structural Properties*, Vol. 18 of *Advances in Physics* (Taylor & Francis, London, 1969).

[3] R. Friendt and A. Yoffe, *Electronic Properties of Intercalation Complexes of the Transition Metal Dichalcogenides*, Vol. 36 of *Advances in Physics* (Taylor & Francis, London, 1987).

[4] J. Phys. C: Solid State Phys. **20**, 4019 (1987).

[5] R. Manzke and M. Skibowski in *Electronic Structure of Solids: Photoemission Spectra and Related Data*, edited by A. Goldmann, Landolt-Börnstein, New Series, Group III, Vol. 23, p. 84 (Springer-Verlag, Berlin, 1994).

[6] A. Koma, K. Sunouchi, and T. Miyajima, in *Proceedings of the 17th International Conference on Physics Semiconductors, San Francisco 1984*, edited by J. Chadi and W. Harrison (Springer, New York, 1984), p. 1465.

[7] A. Koma, Thin Solid Films **216**, 72 (1992).

[8] L. Roubi and C. Carlone, Can. J. Phys. **66**, 633 (1988).

[9] K. Terashima and I. Imai, Solid State Commun. **63**, 315 (1987).

[10] D. L. Greenaway and R. Nitsche, J. Phys. Chem. Solids **26**, 1445 (1965).

[11] C. Y. Fong, J. Camassel, S. Kohn, and Y. R. Shen, Phys. Rev. B **13**, 5442 (1976).

[12] D. W. Bullet, J. Phys. C **11**, 4501 (1978).

[13] R. B. Murray, R. A. Bromley, and A. D. Yoffe, J. Phys. C **5**, 746 (1972).

[14] L. F. Mattheiss, Phys. Rev. B **8**, 3719 (1973).

[15] G. Jakovidis, J. D. Riley, J. Liesegang, and R. C. G. Leckey, J. Electron Spectrosc. Relat. Phenom. **42**, 275 (1986).

[16] M. Skibowski and L. Kipp, J. Electron Spectrosc. Relat. Phenom. **68**, 77 (1994).

[17] L. Kipp, M. Boehme, H. Carstensen, R. Claessen, and M. Skibowski, Rev. Sci. Instrum. **68**, 2144 (1997).

[18] P. W. Erdman and E. C. Zipf, Rev. Sci. Instrum. **53**, 225 (1982).

[19] T. Seydel and F. Wagner (unpublished).

[20] B. Buck and V. A. Macaulay, *Maximum Entropy in Action, ACollection of Expository Essays* (Clarendon, Oxford, 1991).

[21] R. Manzke, H. Barnscheidt, C. Janowitz, and M. Skibowski, Phys. Rev. Lett. **58**, 610 (1987).

[22] L. Kipp, R. Manzke, and M. Skibowski, Proc. SPIE **1361**, 794 (1991).

[23] L. Kipp, R. Manzke, and M. Skibowski, Solid State Commun. **93**, 603 (1995).

[24] M. Traving, M. Boehme, L. Kipp, M. Skibowski, F. Starrost, E. E. Krasovskii, A. Perlov, and W. Schattke, Phys. Rev. B **55**, 10 392 (1997).

[25] Optical measurements by the authors on HfS_2, 1999.

[26] O. K. Andersen, Phys. Rev. B **12**, 3060 (1975).

[27] V. V. Nemoshkalenko, A. A. Krasovsky, V. N. Antonov, V. N. Antonov, U. Fleck, H. Wonn, and P. Ziesche, Phys. Status Solidi B **120**, 283 (1982).

[28] E. E. Krasovskii and W. Schattke, Solid State Commun. **93**, 775 (1995).

[29] E. E. Krasovskii, Phys. Rev. B **56**, 12 866 (1997).

[30] V. N. Antonov, A. I. Bagljuk, A. Y. Perlov, V. V. Nemoshkalenko, V. N. Antonov, O. K. Andersen, and O. Jepsen, Low Temp. Phys. **19**, 494 (1993).